Neuron
Article

Distinct Roles of TRP Channels in Auditory Transduction and Amplification in *Drosophila*

Brendan P. Lehnert,[1] Allison E. Baker,[1] Quentin Gaudry,[1] Ann-Shyn Chiang,[2] and Rachel I. Wilson[1,*]
[1]Department of Neurobiology, Harvard Medical School, 220 Longwood Avenue, Boston, MA 02115, USA
[2]Department of Life Science, National Tsing Hua University, Hsinchu 30013, Taiwan
*Correspondence: rachel_wilson@hms.harvard.edu
http://dx.doi.org/10.1016/j.neuron.2012.11.030

SUMMARY

Auditory receptor cells rely on mechanically gated channels to transform sound stimuli into neural activity. Several TRP channels have been implicated in *Drosophila* auditory transduction, but mechanistic studies have been hampered by the inability to record subthreshold signals from receptor neurons. Here, we develop a non-invasive method for measuring these signals by recording from a central neuron that is electrically coupled to a genetically defined population of auditory receptor cells. We find that the TRPN family member NompC, which is necessary for the active amplification of sound-evoked motion by the auditory organ, is not required for transduction in auditory receptor cells. Instead, NompC sensitizes the transduction complex to movement and precisely regulates the static forces on the complex. In contrast, the TRPV channels Nanchung and Inactive are required for responses to sound, suggesting they are components of the transduction complex. Thus, transduction and active amplification are genetically separable processes in *Drosophila* hearing.

INTRODUCTION

Mechanosensation is fundamental to all living organisms. However, the molecular identity of the channels that convert force into electrical current has been largely a matter of conjecture. Moreover, the molecular and cellular mechanisms that modulate the forces acting on these mechanosensitive channels are also poorly understood.

Studies in *Drosophila melanogaster* have made important contributions to our understanding of mechanosensation. In particular, a genetic screen in *Drosophila* identified the first member of the transient receptor potential (TRP) family to be implicated in mechanosensation (Robert and Hoy, 2007; Walker et al., 2000). That TRP channel—dubbed NompC or TRPN1—is thought to be a component of the transduction complex that converts mechanical force into an electrical signal in *Drosophila* auditory receptor neurons (Effertz et al., 2012; Effertz et al., 2011; Göpfert et al., 2006; Kamikouchi et al., 2009; Lee et al., 2010; Liang et al., 2011). Auditory receptor neurons in *Drosophila* are termed Johnston's organ neurons (JONs), and are housed in the antenna. Sound stimuli cause the distal segment of the antenna to rotate on its long axis, and this rotation transmits forces into the more proximal portion of the antenna, just as rotating a key transmits force to a lock. This stretches JON dendrites, opening mechanosensitive channels (Göpfert and Robert, 2002; Göpfert and Robert, 2001; Kernan, 2007).

Multiple lines of evidence support the idea that NompC has a key role in mechanotransduction. Loss of the *C. elegans* homolog eliminates force-gated receptor currents in mechanosensitive cephalic neurons, and amino acid substitutions in the putative pore domain of the *C. elegans* channel can alter the ionic sensitivity of receptor currents (Kang et al., 2010). In *Drosophila* larvae, loss of NompC eliminates calcium signals in multidendritic mechanosensory neurons in the body wall during crawling (Cheng et al., 2010). In adult *Drosophila*, loss of NompC reduces sound-evoked electrical activity in the antennal nerve (Eberl et al., 2000; Effertz et al., 2012; Effertz et al., 2011), as well as evoked potentials in mechanosensitive bristles (Walker et al., 2000).

NompC has a particularly interesting role in the mechanics of the *Drosophila* antenna. Normally, motile elements in the auditory organ expend energy in order to augment sound-evoked motion (Göpfert et al., 2005). This process is called active amplification. Loss of NompC abolishes active amplification in the *Drosophila* antenna (Göpfert et al., 2006; Göpfert and Robert, 2003). Active amplification also exists in vertebrate hair cells, and a component of active amplification is linked to the gating of hair cell mechanotransduction channels (Hudspeth, 2008). By analogy with hair cells, active amplification in *Drosophila* has been proposed to depend directly on transduction channel gating (Nadrowski et al., 2008). NompC has been proposed to play a direct role in transduction chiefly because it is required for sound-evoked active amplification (Göpfert et al., 2006) and is also required for the normal mechanical compliance of the antenna in response to a force step (Effertz et al., 2012). However, loss of NompC does not entirely eliminate sound-evoked field potentials in the *Drosophila* auditory nerve (Eberl et al., 2000; Effertz et al., 2011, 2012), leading to the speculation that another gene might play a redundant function.

Two additional *Drosophila* TRP channels—Nanchung and Inactive—are also expressed in auditory receptor neurons (Gong et al., 2004; Kim et al., 2003), and likely function as a heteromer (Gong et al., 2004). These TRPV family members are not thought to be part of the transduction complex, because they localize to a subcellular region that is several microns away

from the region occupied by NompC (Cheng et al., 2010; Gong et al., 2004; Lee et al., 2010; Liang et al., 2011). Nevertheless, both Nanchung and Inactive are required for sound-evoked field potentials in the antennal nerve, which houses the axons of JONs (Gong et al., 2004; Kim et al., 2003). These potentials are thought to reflect mainly spike-mediated currents in JONs. Thus, it has been proposed that Nanchung and Inactive are required to amplify subthreshold electrical signals generated by the transduction complex, thereby producing signals large enough to elicit spikes in JONs (Göpfert et al., 2006; Kamikouchi et al., 2009; Lee et al., 2010).

That said, it is not clear how Nanchung/Inactive might amplify a signal generated by the transduction complex. Amplification by second messengers is unlikely because these processes are much slower than the auditory transduction latency (Albert et al., 2007; Eberl et al., 2000). Electrical amplification also seems unlikely, as Nanchung and Inactive form channels in heterologous cells that are only weakly voltage-dependent (Gong et al., 2004; Kim et al., 2003).

A primary difficulty in resolving the roles of the TRP channels implicated in *Drosophila* auditory transduction has been the fact that recordings from individual auditory receptor neurons are not feasible. This is because JONs are very small cells embedded in a delicate antennal organ whose integrity is critical to their function. Thus, we lack any electrophysiological measure finer than field potential recordings from the auditory nerve.

Finally, the problem is compounded by the fact that the field lacks a consensus regarding what stimuli fall within the dynamic range of the *Drosophila* auditory system. On the one hand, active amplification of antennal motion can be observed in response to relatively weak sound stimuli (as low as 26 dB SVL; Göpfert et al., 2006). If active amplification is the hallmark of transduction, then *Drosophila* auditory sensitivity might rival that of humans. On the other hand, behavioral measures of auditory sensitivity suggest that *Drosophila* have a comparatively high threshold for hearing, variously reported as 92 dB (von Schilcher, 1976) or ~72 dB (Eberl et al., 1997; Inagaki et al., 2010).

In this study, we aimed to clarify these issues in three ways. First, we developed a novel behavioral assay to measure the sensitivity of *Drosophila* hearing, thereby establishing an upper bound for the most sensitive neural threshold that must exist among JONs. Second, we developed a non-invasive method for monitoring sound-evoked subthreshold signals in JONs. Third, using this recording method, together with genetic manipulations of transduction and spiking in JONs, we assessed the relative roles of TRP family members in specifying the sensitivity of auditory transduction. Our results show that Nanchung and Inactive are required for sound-evoked subthreshold signals in JONs. By contrast, NompC is not required for mechanotransduction, and indeed transduction can reach normal peak levels in the absence of NompC. Rather, our results imply that NompC modulates the forces that gate the transduction complex.

RESULTS

Drosophila Hearing Is Sensitive to Low-Intensity Sounds

Prior electrophysiological, mechanical, and behavioral measures have led to different impressions of the sensitivity of the *Drosophila* auditory system (Eberl et al., 1997; Göpfert et al., 2006; Inagaki et al., 2010; Kernan, 2007). Therefore, we began by asking what sound intensities elicit a behavioral response. Behavioral measurements are important because they set an upper bound on the neural threshold.

Almost all studies to date have measured behavioral thresholds in the context of courtship, under conditions where it is difficult to precisely control the intensity of stimulation. We reasoned that a simple acoustic startle reflex might yield lower estimates of the threshold. We tethered flies and suspended them above a small plastic ball floating on a cushion of air (Figure 1A). The fly's fictive running was measured by optically monitoring the movement of the ball. Calibrated sound stimuli were delivered from a speaker in front of the fly. In this apparatus, the flies tended to run spontaneously, alternating with brief bouts of standing still. In response to tone pips, the fly tended to transiently stop their forward running (Figure 1B).

We observed startle behavior in response to sounds with an intensity as low as 1.2×10^{-4} m/s, or 65 dB SVL (Figure 1C). This threshold is lower than that estimated previously using courtship behaviors (Eberl et al., 1997; Inagaki et al., 2010; Kernan, 2007) and is similar to that recently reported using a conditioned proboscis response reflex (Menda et al., 2011). This result means that the most sensitive JONs must have thresholds at or below this intensity. It also demonstrates that these intensities are behaviorally relevant.

We verified that startle behavior was abolished when we stabilized the most distal antennal segment with a drop of glue (Figure 1D). It was also attenuated when we suppressed spiking in JONs by selective RNAi-mediated knockdown of voltage-dependent sodium channels (Nagel and Wilson, 2011) under the control of a JON-specific Gal4 line (Figure 1E). Thus, the startle behavior requires sound-evoked spiking in JONs.

As an initial measurement of neural thresholds, we made field potential recordings from the antennal nerve. Sounds elicited field potential oscillations at twice the stimulus frequency (Figure 1F), as previously reported (Eberl et al., 2000). For the 300 Hz tone, 5.7×10^{-5} m/s (58 dB SVL) was the lowest intensity that elicited a response significantly above the response to background noise (Figure 1G; $p < 0.05$, t test, $n = 6$). As expected, the neural threshold is lower than the behavioral threshold.

We also used laser Doppler vibrometry to measure the sound-evoked rotational movement of the antenna. In agreement with previous studies (Göpfert et al., 2006; Göpfert and Robert, 2003), we observed a nonlinearity in the antenna's movement as sound intensity increased. Specifically, antennal rotations (normalized to sound intensity) were largest for low-intensity sounds, and became smaller for high-intensity sounds (Figure 1G). This phenomenon is consistent with active amplification of movements produced by weak sounds (Göpfert et al., 2005). It is notable that active amplification is observable for intensities below the threshold for antennal field potential responses (Figure 1G). This suggests that active amplification may be a process distinct from transduction, rather than being a hallmark of transduction, and motivates the need for a sensitive measure of JON activity.

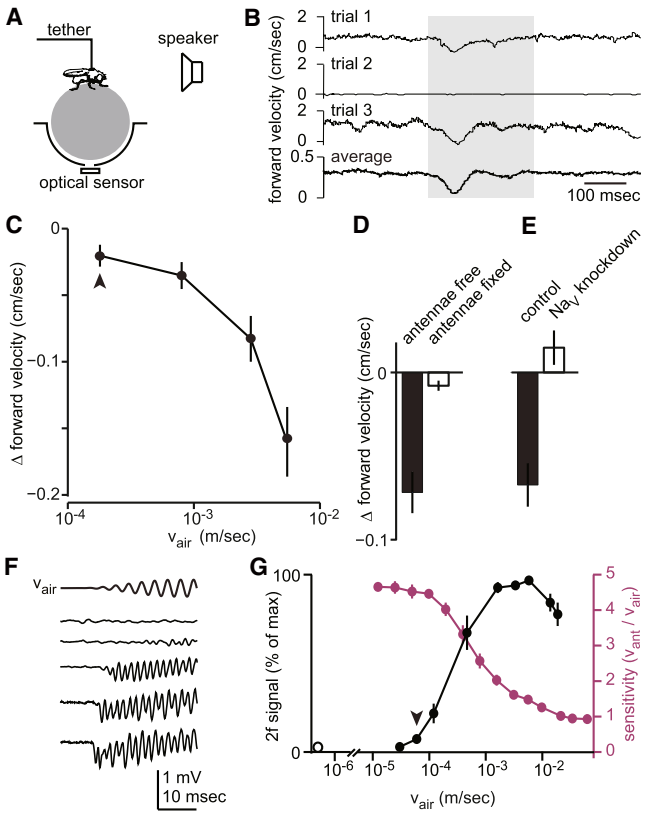

Figure 1. *Drosophila* Hearing Is Sensitive to Low-Intensity Sounds

(A) Measurement of the acoustic startle response. A tethered fly faces a speaker while standing on a spherical treadmill.

(B) The fly's fictive forward velocity plotted versus time. The gray box represents the time of the sound stimulus (300 Hz tone, played at an intensity of 0.0055 m/s). Shown are three individual trials (in one of which the fly was not moving), plus an average of 27 trials for this condition.

(C) Responses to sound grow with sound intensity. Arrowhead indicates the lowest intensity where the forward velocity during the tone was significantly different from the forward velocity immediately prior to the tone (mean ± SEM; $p < 0.05$, paired t test with sequential Bonferroni correction, n = 19–27 flies).

(D) Fixing the antenna in place with adhesive reduces the behavioral response to sound ($p < 0.0005$, t test, n = 19 free and 7 fixed). Within each fly, the responses to all stimulus intensities were averaged together prior to statistical testing, and SEM was computed across flies on this averaged data.

(E) Selective RNAi-mediated knockdown of voltage-gated sodium channels in JONs reduces the response to sound ($p < 0.01$, t test, n = 11 control and 11 knockdown). As in (D), responses were averaged across all stimulus intensities.

(F) Field potential recordings from the antennal nerve in response to ramped 300 Hz tones of increasing sound intensity (corresponding to every other intensity in G). The acoustic particle velocity waveform recorded in the vicinity of the fly (v_{air}) is shown at top.

(G) The field potential response (quantified as the signal at twice the sound frequency, normalized to the maximum in each experiment) is plotted as a function of sound intensity (black circles). The open black circle shows the background noise at 300 Hz in the vicinity of the preparation and the corresponding field potential. Arrowhead indicates the response to the least intense sound that was significantly different from the response to background (mean ± SEM; $p < 0.05$, Wilcoxon rank-sum tests with sequential Bonferroni correction). The sensitivity of antennal rotational movement is also shown as a function of sound intensity (magenta). Sensitivity is computed as the ratio of antennal angular velocity (in radians/s) to acoustic particle velocity amplitude (in m/s).

Spikes from Auditory Receptor Neurons Propagate into the Giant Fiber Neuron through Gap Junctions

Attempts to record directly from individual JONs were unsuccessful due to the fact that these are small cells embedded in a delicate auditory organ. We therefore developed a method for recording signals noninvasively from JONs, with the ultimate goal of recording the signals that give rise to action potentials. We reasoned that we might be able to achieve this by recording from the giant fiber neuron (GFN), a single identifiable central neuron that extends dendrites into the region of the brain where JON axons terminate (Figure 2A; Kamikouchi et al., 2009). A recent study has shown that the GFN responds to auditory stimuli (Tootoonian et al., 2012). What distinguishes the GFN from other central auditory neurons is the finding that dye loaded into JONs can diffuse directly into the GFN, implying that it is coupled to the JON by gap junctions (Strausfeld and Bassemir, 1983). Consistent with this, electron microscopy has shown that JON axons form gap junctions with cells in the vicinity of the GFN dendrites (Sivan-Loukianova and Eberl, 2005). Thus, we made in vivo whole-cell patch-clamp recordings from the GFN to ask whether it receives direct electrical input from JONs via gap junctions. We made these recordings in voltage-clamp configuration to minimize cable filtering by the GFN dendrite, and to minimize the contribution of active conductances in the GFN. To target our electrodes to the GFN, we used specific Gal4 lines to drive GFP expression in this neuron.

In the absence of sound stimuli, we observed hundreds of spontaneous excitatory events in the GFN (Figure 2B) every second. Events that were well-isolated in time had a stereotyped profile within a fly and across flies, and were very fast (<1 ms half-width; Figure 2C). Pure tone stimuli caused excitatory currents to arrive in oscillatory bursts at twice the sound frequency (Figure 2B). This is similar to the frequency doubling observed in the antennal nerve field potential. When we prevented the distal antennal segment from rotating by fixing it with a drop of glue, we observed that spontaneous events persisted, but the response to sound was abolished (Figures 2B). Removing the antennae eliminated both spontaneous events and sound responses (Figures 2B). These results imply that spontaneous events arise in antennal neurons and—because they are modulated by sound—likely originate in JONs. The speed and stereotypy of these events suggest that they represent action potentials in JONs which then propagate into the GFN via gap junctions. (Note that, whereas we are voltage-clamping the GFN, we are unlikely to be voltage-clamping JONs across these gap junctions. This means that action potentials can arise in JONs and propagate across the gap junctions.)

We used pharmacological and genetic manipulations to verify that these events are JON spikes which propagate across gap junctions. We confirmed that blocking chemical synaptic transmission with bath application of Cd^{2+} had no effect (Figures 2D and 2E), although this manipulation blocks chemical synaptic transmission in the *Drosophila* olfactory system (Kazama and Wilson, 2008). We also confirmed that spontaneous events in the GFN were abolished by blocking spikes throughout the brain with bath application of tetrodotoxin (TTX). Similarly, events were virtually eliminated by RNAi-mediated knockdown

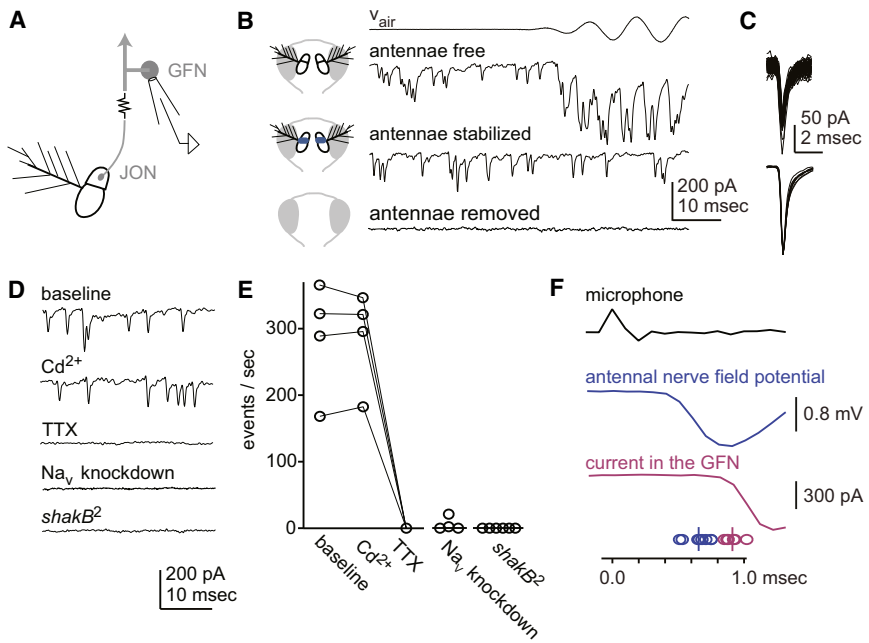

Figure 2. Spikes from Auditory Receptor Neurons Propagate into the Giant Fiber Neuron through Gap Junctions

(A) Schematic showing a Johnston's organ neuron (JON) in the antenna whose axon projects into the brain and is connected via gap junctions with the dendrite of the Giant Fiber Neuron (GFN). The GFN sends an axon into the thorax (arrow). In vivo whole-cell patch clamp recordings were made from the GFN soma.

(B) Spontaneous and evoked currents recorded in the GFN during presentation of a sound stimulus (100 Hz, 0.0024 m/s). Stabilizing the antennae by gluing the distal (third) antennal segment to the more proximal (second) segment abolishes sound responses but not spontaneous events. Removing the antennae abolishes both spontaneous events and sound responses.

(C) Well-isolated spontaneous events show a stereotyped shape and size (top, same cell as in B). The average shape of these events is also stereotyped across cells (bottom, 9 average events scaled to the same peak).

(D) Representative recordings show that, relative to baseline, event rates are unaffected by pharmacological blockade of chemical synapses (200 μM Cd^{2+}) but abolished by blocking spiking (2 μM TTX) and greatly reduced by selective transgenic knockdown of voltage-gated sodium channels in JONs. Recorded events are also abolished by a mutation in the gap junction subunit *shakB*.

(E) Group data showing the rate of spontaneous events for each manipulation. Each circle is a different experiment, and lines connect measurements from the same experiment. All manipulations produce a significant reduction ($p < 0.05$, paired or unpaired Wilcoxon rank-sum tests with Bonferroni correction), except for Cd^{2+}.

(F) A click stimulus elicits a microphonic potential in the vicinity of the fly (top), followed rapidly by a field potential deflection in the antennal nerve (blue) and an inward current in the GFN (magenta). Neural responses are averages of 50–100 trials. Latencies from click arrival (calculated as the time when the response reached 10% of maximal) are shown for all antennal nerve ($n = 7$) and GFN recordings ($n = 6$) at bottom. The delay between the average field potential latency and average GFN latency is 271 μs. This value includes the time required for the electrical signal to propagate from the antenna (where the field potential is recorded) down the antennal nerve and into the brain.

of voltage-gated sodium channels selectively in JONs (Figures 2D and 2E). Finally, events were abolished by a null mutation in the gap junction subunit *shakB* (Figures 2D and 2E; Curtin et al., 2002; Phelan et al., 1996).

Together, these findings are strong evidence that events are individual JON spikes, rather than synaptic events. These results also demonstrate that the events propagate into the GFN via electrical synapses. Consistent with the conclusion that these synapses are electrical, there is a delay of <300 μs from JON spiking to the onset of currents in the GFN (Figure 2F).

Subthreshold Signals from Auditory Receptor Neurons Propagate into the Giant Fiber Neuron

Next we asked whether we could use GFN recordings as a way to monitor the subthreshold signals in JONs that give rise to spikes. To block spikes, we bath-applied TTX, which reduced sound-evoked currents to about 5% of their original level (Figure 3A). In experiments where we selectively knocked down voltage-gated sodium channels in JONs, we observed sound-evoked currents similar to those recorded in wild-type flies with TTX in the bath (Figures 3B and 3C). This argues that the effect of TTX on the sound-evoked currents is due to the blockade of spiking JONs. The currents recorded in TTX thus reflect the subthreshold depolarization in JONs that normally gives rise to JON spikes. The subthreshold depolarization propagates through gap junctions into the GFN, where it gives rise to currents in our voltage-clamp recording. We will use the term "generator currents" to refer to the currents we record in the GFN in the presence of TTX.

Both spike-mediated currents and generator currents were sensitive to weak sound intensities (Figures 3D and 3E). Notably, whereas the spike-mediated currents declined at high intensities, the generator currents showed a smooth monotonic dependence on sound intensity. This indicates that the decline in the spike-mediated currents is due to spike rate adaptation, and not adaptation in transduction. Also, whereas spike-mediated currents were selective for the frequency of the sound stimulus (with higher frequencies producing smaller responses), the generator currents were less so. This suggests that some of the frequency selectivity in spike-mediated currents is due to an inability to generate spikes efficiently at high pitches, again probably due to spike rate adaptation.

Next, we asked how transduction depends on antennal rotation. We measured rotations in response to these sound stimuli using laser Doppler vibrometry (see Figure S1 available online). We used these measurements to plot generator currents as a function of antennal rotation (Figure 3F). These plots show that different sound stimuli generated the same monotonic curve, regardless of frequency. This indicates that the apparent frequency selectivity of the generator currents is due to the

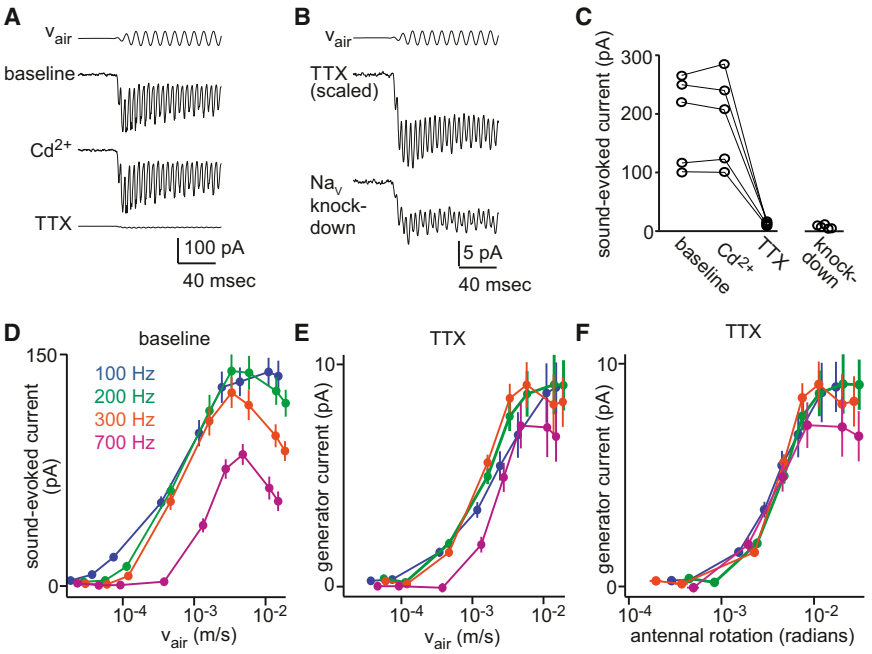

Figure 3. Subthreshold Signals from Auditory Receptor Neurons Propagate into the Giant Fiber Neuron

(A) Sound-evoked currents from a representative experiment. All traces are averages of 50–100 trials, and thus spontaneous activity is averaged out, leaving only the sound-locked response. Blocking chemical synapses (200 μM Cd^{2+}) had no effect, but blocking spikes (2 μM TTX) reduced sound-evoked currents by ~95%. The stimulus is a 100 Hz tone (0.0024 m/s).

(B) Sound-evoked generator currents. The recording in TTX (top) is the same as in A, but displayed on an expanded vertical scale. In a recording where voltage-gated sodium channels were selectively knocked down in JONs (bottom), the result is similar to bath application of TTX. The dynamics of the generator current resemble the dynamics of the spike-mediated current in (A) for this stimulus; however, spike-mediated currents show more accommodation than generator currents when the stimulus is a higher-frequency tone.

(C) Group data showing the magnitude of currents recorded in response to a 100 Hz tone (0.0024 m/s) for each manipulation. Each circle is a different experiment, and lines connect measurements from the same experiment.

(D) Sound-evoked currents (mean ± SEM; recorded in the absence of TTX) as a function of sound intensity (n = 8).

(E) Sound-evoked generator currents (recorded in TTX) as a function of sound intensity (n = 8). Note that TTX eliminates the decrease in responses at high sound intensity, indicating that this decrease is likely due to spike adaptation in JONs.

(F) Sound-evoked generator currents (recorded in TTX) plotted against sound-evoked antennal rotation (same experiments as in E). Note that frequency tuning is essentially eliminated.

See also Figure S1.

frequency selectivity of the antenna, which has a resonant frequency around 160–300 Hz at low sound intensities (Göpfert and Robert, 2002, 2003). When we combined data from these two types of measurements to construct a current-rotation curve, it becomes clear that there is a single relationship between transduction and antennal movement. In the remainder of this study, we will focus on how TRP channels specify this relationship.

Loss of Nanchung or Inactive Abolishes Generator Currents

It has been proposed that Nanchung and Inactive amplify subthreshold transduction currents to the level of spike initiation (Göpfert et al., 2006; Kamikouchi et al., 2009; Lee et al., 2010). If so, then we should be able to measure generator currents in *nanchung* and *inactive* mutant flies. Contrary to this prediction, we found that both spike-mediated sound responses and sound-evoked generator currents were completely absent in null mutants of either gene (nan^{36a} and iav^{1}) (Figures 4A and 4B). The rate of spontaneous events was drastically reduced in both mutants, but events still had a normal size and shape (Figure 4A). This result suggests that these TRPV channels are required for a resting conductance that drives spontaneous JON spiking, but it also demonstrates that neither TRPV is required for JON spikes per se.

We observed no sound-evoked generator current in either mutant at any sound intensity in our test set. The meaningfulness of this observation depends critically on the sensitivity of our measurement, so we examined the recorded currents in the frequency domain where we expect signal detection to be optimal. The frequency representation shows a prominent peak at twice the frequency of the sound stimulus in wild-type recordings, but there is no corresponding peak in recordings from the TRPV mutants at this frequency (Figure 4C). Focusing on a narrow band around this frequency, we calculated the signal gain over background noise for the currents recorded in TTX. On average, the signal gain was >110-fold in wild-type, and indistinguishable from zero in both mutants (Figure 4D). If Nanchung and Inactive serve to amplify the transduction signal, then they would need to amplify that signal at least 110-fold to escape detection. If NompC were an essential component of the transducer, one might imagine that these phenotypes could arise if NompC were trafficked improperly in these mutants; however, we confirmed that NompC localizes correctly even in the absence of Nanchung (Figure 4E).

Spikes and Generator Currents Arise from an Identified Genetic Population of Receptor Neurons

JONs were initially subdivided into types based on the observation that groups of JONs project to different brain regions (Kamikouchi et al., 2006). Calcium imaging studies have subsequently shown that type AB JONs have a lower threshold for sound stimuli than type CE JONs (Effertz et al., 2011; Kamikouchi et al., 2009). A calcium imaging study has also reported that NompC is absolutely required for sound responses in type AB

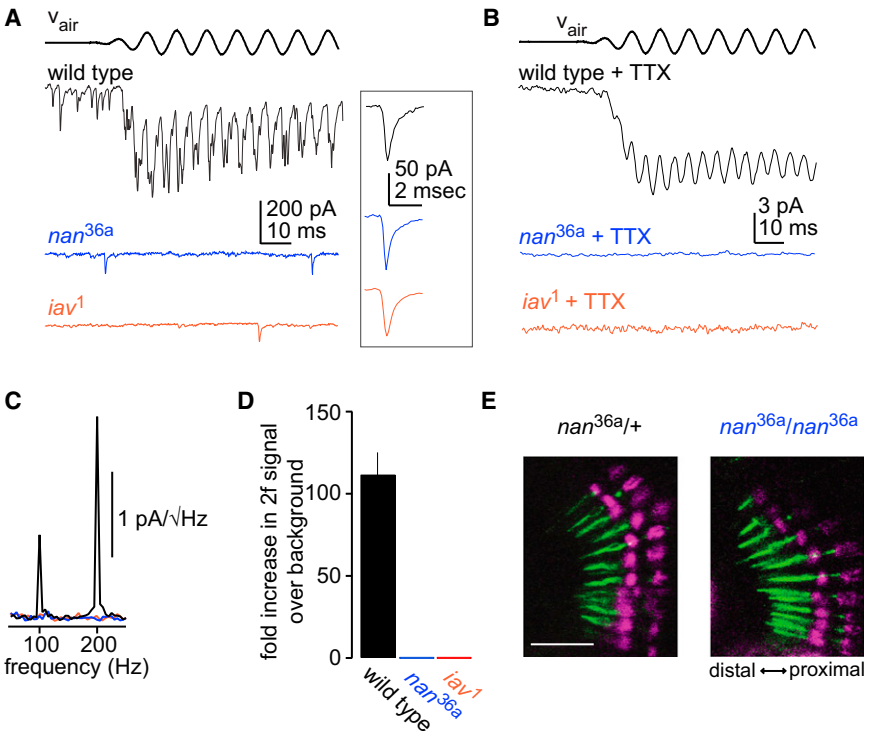

Figure 4. Loss of Nanchung or Inactive Completely Abolishes Generator Currents

(A) Single trials showing currents recorded in the GFN in response to a 100 Hz tone (0.0044 m/s). In the *nanchung* and *inactive* mutants, sound responses are absent. Spontaneous events are greatly reduced in frequency as compared to wild-type, but when they occur, their size and shape is similar to wild-type. Insets (right) show the average shape and size of the isolated events in these recordings.

(B) Representative generator current recordings in the presence of TTX. Traces are averages of 100–500 trials. Generator currents are absent in the *nanchung* and *inactive* mutants. The sound stimulus is the same as in (A). Note the expanded current scale.

(C) Frequency domain representation of the generator currents in (B). The wild-type currents show a large peak at twice the sound frequency (2f) and a smaller peak at the frequency of sound stimulation (1f). The currents in both mutants show no measurable peak at 1f or 2f.

(D) Mean signal (±SEM) at twice the sound frequency (2f) as a fold change over that present in a baseline period of equivalent length (n = 18 wild-type, 5 *nanchung* mutants, 5 *inactive* mutants).

(E) Confocal immunofluorescent images of JONs within the second antennal segment. An antibody that localizes to the ciliary dilation (21A6, magenta) marks the boundary between the distal and proximal dendrite of each JON. A NompC:GFP fusion protein (green) localizes properly to the distal portion of the dendrite in both genotypes, showing loss of Nanchung does not disrupt NompC localization. Images are *z*-projections through an 8 μm-depth, scale bar is 10 μm.

JONs, whereas NompC is dispensable for sound responses in CE JONs (Effertz et al., 2011). Although the available evidence suggests that all JONs express NompC, Nanchung, and Inactive (Cheng et al., 2010; Gong et al., 2004; Lee et al., 2010), it remains possible that these TRPs might play different roles in different JON types (Effertz et al., 2011, 2012; Kamikouchi et al., 2009).

Given these considerations, we sought to clarify which JON types give rise to the signal that we record in the GFN. First, we filled the GFN with a biocytin marker in flies where distinct classes of JON axons were labeled with GFP. The GFN dendrite is likely to directly contact some JONs, given the short latency of the GFN response to sound stimuli (Figure 2F). Indeed, we observed apparent contacts between the GFN dendrite and type AB JONs, but no contacts for type CE JONs (Figure 5A). These results confirm an earlier study showing that the GFN dendrites arborize in the region where type AB axons terminate (Kamikouchi et al., 2009).

We next tested whether the GFN is functionally connected solely to type AB JONs, or whether type CE JONs also provide input to the GFN. This could be the case if an indirect connection existed between type CE JONs and the GFN. We created flies where just one of the two types of JONs is functional, by virtue of cell-specific rescue of *inactive* in an *inactive* mutant background. As a positive control, we confirmed that rescuing *inactive* expression in most or all JONs was able to rescue the mutant phenotype in GFN recordings (Figures 5B and 5C). When we rescued *inactive* selectively in type AB JONs, we also observed complete rescue, and these recordings were indistinguishable from wild-type or pan-JON rescue (Figures 5B and 5C). By contrast, rescuing *inactive* selectively in type CE JONs had no effect, equivalent to flies where the Gal4 driver was omitted (Figures 5B and 5C). Thus, the signals we record in the GFN arise exclusively in type AB JONs.

These results also place an upper bound on the number of JONs providing input to the GFN. The Gal4 line we used to rescue type AB JONs is expressed in a total of 145 neurons in each JO (Inagaki et al., 2010). Because this line produced complete rescue, our recorded signals arise from this number of JONs, or a subset thereof.

Loss of NompC Decreases the Sensitivity of Generator Currents to Antennal Rotation

We next examined generator currents in a mutant that lacks functional NompC (specifically, $nompC^3/nompC^1$ *trans*-heterozygotes; Walker et al., 2000). Sound stimuli still evoked generator current in the *nompC* mutant, meaning that transduction is still present in the type AB JONs that provide input to the GFN. However, responses were systematically smaller than normal (Figure 6A). Sound-induced antennal rotations were also smaller in *nompC* mutants at some of these particle velocities, due to a loss of active amplification (Göpfert et al., 2006), so we controlled for this by measuring sound-evoked antennal movements in wild-type flies and mutants, and plotting the sound response data relative to antennal rotations. This showed that currents in *nompC* mutants are smaller even if we control for the size of antennal rotations (Figure 6B), and this

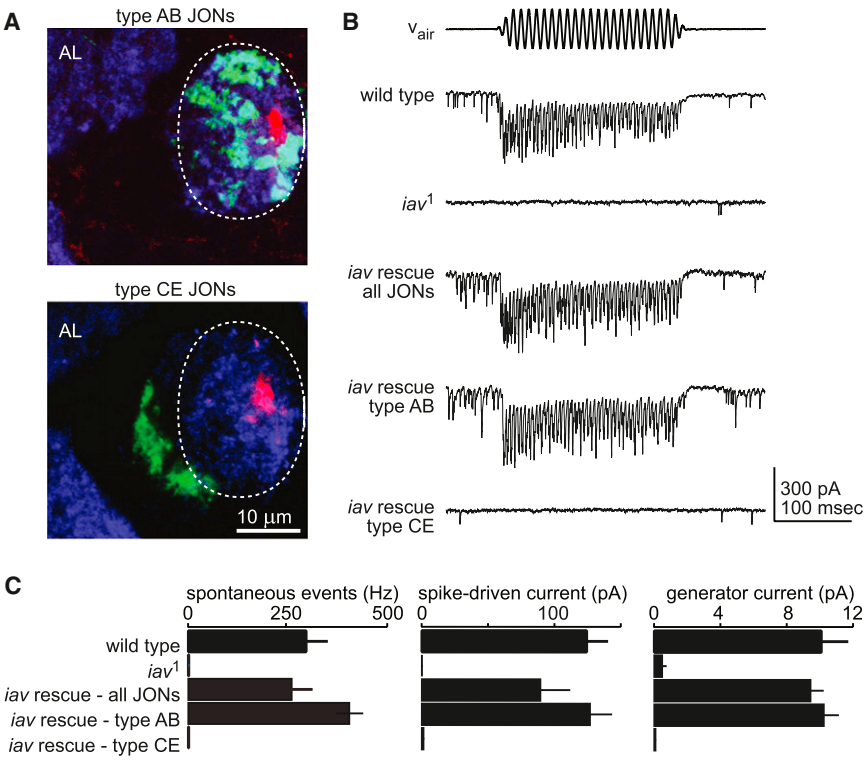

Figure 5. Spikes and Generator Currents Arise from an Identified Genetic Population of Receptor Neurons

(A) Confocal immunofluorescent images of JON axons (green) and the GFN dendrite (red). The GFN colocalizes with axons of JON-AB axons but not JON-CE axons. JONs are labeled with CD8:GFP and the GFN dendrite is filled with biocytin from the recording pipette. (In these recordings, the GFN was patched without labeling it with GFP.) An antibody against a synaptic antigen (nc82, blue) stains the synapse-rich part of the antennal mechanosensory and motor center (dotted ellipse) and the antennal lobe (AL). Images are *z*-projections through a 3-μm depth. Inspection of the entire confocal stack showed multiple points of contact between labeled JONs and the GFN.

(B) Representative single trials showing spontaneous events and spike-mediated sound responses in wild-type and *inactive* mutant flies, as well as in flies where *inactive* is rescued in all JON types (under the control of *nanchung-Gal4*), in type AB JONs (under the control of *JO-AB-Gal4*), and in type CE JONs (under the control of *JO-CE-Gal4*). The sound stimulus is a 100 Hz tone at 0.0044 m/s.

(C) Rescue of *iav* in type AB JONs is sufficient to completely restore spontaneous events, spike-mediated sound responses, and generator current sound responses (mean ± SEM). There is a difference in the mean values of all three metrics across groups (one-way ANOVA, $p < 0.001$ for all three measures). The mean values of all three metrics are not significantly different between wild-type, all-JON rescue, and type AB rescue (Tukey's HSD, $p > 0.05$, n = 4, 5, and 6). Similarly, the values of all three metrics are not significantly different in type CE rescue and the *iav* mutants (Tukey's HSD, $p > 0.05$, n = 6 for rescue in CE, 4 for *iav* mutants). There is a significant difference in all three metrics between the members of these two subsets.

was consistent across a range of sound frequencies (data not shown). This implies that the loss of NompC reduces the sensitivity of the transduction complex to antennal rotation.

In *nompC* mutants, the maximal amplitude of the sound-evoked currents that we recorded was lower than wild-type levels (Figure 6B). However, *nompC* mutant responses to sound stimuli did not saturate, and so the true maximum amplitude is not clear from these recordings. Therefore, we extended our observations by measuring generator currents while using a rigid, piezoelectrically-actuated probe to rotate the distal antennal segment. In this recording configuration, step rotations produce short-latency currents which decay over tens of milliseconds; the rapid adaptation to the static step is further evidence that the GFN is postsynaptic to the fast-adapting AB JONs and not the slow-adapting CE JONs (Kamikouchi et al., 2009). Step rotations of the antenna produce currents which increase monotonically with step amplitude and saturate for the largest steps (Figures 6C and 6D).

In the *nompC* mutants, responses to small steps were systematically weaker as compared to wild-type (Figures 6C and 6D). For small steps, the rise time was also slower in the *nompC* mutant than in wild-type. In effect, mutant responses are similar to wild-type responses to smaller steps, suggesting that the transduction complex is experiencing less force than normal. Importantly, however, the rise time and amplitude of the currents evoked by the largest steps were essentially identical in both genotypes (Figures 6C–6E). These results imply that NompC does not alter properties inherent to the transduction channels. Rather, NompC is required for normal sensitivity of the transduction complex to antennal movement.

Loss of NompC Does Not Prevent Adaptation

In general, the sensitivity of transduction relies on the existence of adaptation. During a sustained displacement, adaptation shifts the operating range of the system so that it maintains maximal sensitivity (Albert et al., 2007; Fettiplace and Ricci, 2003). We therefore wondered if adaptation was normal in the *nompC* mutant. To investigate this, we again used the piezoelectric probe to apply steps of various amplitudes. Steps in either the medial or lateral direction produced generator currents (Figures 7A and 7B). This is probably because type AB JONs are stretched by both medial and lateral steps (Figure S2).

To measure adaptation, we applied test steps either from a starting point corresponding to the antenna's resting position, or from a new starting point that was offset from the resting position. We chose an offset step that was large enough to evoke a nearly-saturating generator current (Figure 7A). We observed that, within <30 ms after the offset step, currents had regained sensitivity to small rotations in both directions (Figures 7A and 7B). In other words, the region of maximal sensitivity to rotation was recentered around the new static position (Figure 7B). This implies that the lateral and medial resting forces on the transduction complex have been re-equalized.

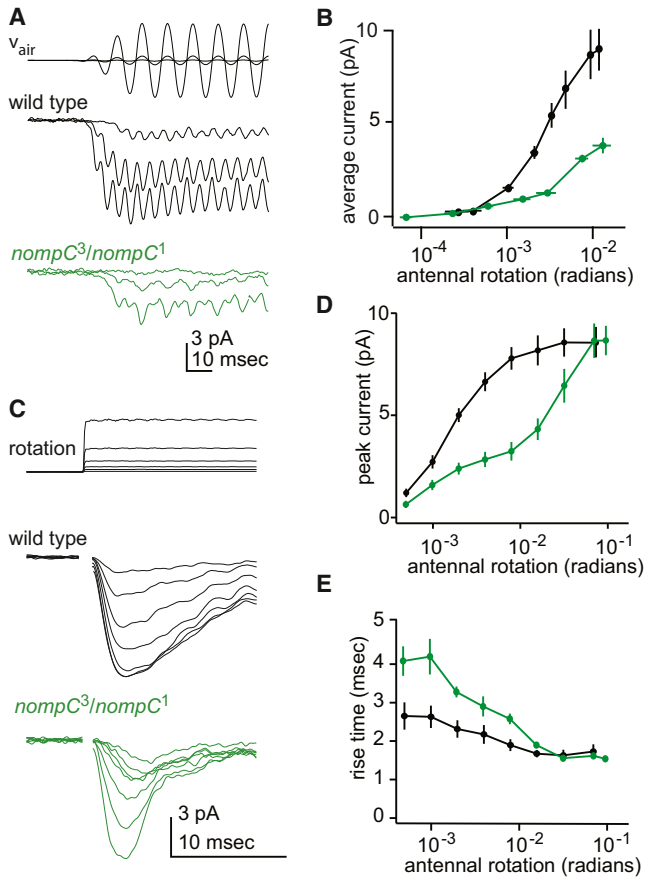

Figure 6. Loss of NompC Decreases the Sensitivity of Generator Currents to Antennal Rotation

(A) Generator currents recorded in response to sound stimuli (100 Hz tones at 0.00034, 0.0024, 0.011 m/s). Acoustic particle velocity (v_{air}) is shown at top; note that the lowest-intensity sound stimulus cannot be seen on this scale. Traces are averaged across all cells recorded in each genotype (n = 9 wild-type, 9 *nompC*^{3}/*nompC*^{1}). (Note that currents in *nompC* mutants oscillate predominantly at the sound frequency, in contrast to wild-type currents that oscillate at twice this frequency; this is characterized in detail below.)

(B) Average generator currents (mean ± SEM) plotted versus the amplitude of antennal rotations evoked by a 100 Hz tone stimulus (n = 9 wild-type, 9 *nompC*^{3}/*nompC*^{1}).

(C) (Top) Piezoelectric step stimuli (lateral steps producing rotations of 0.0005–0.032 radians), measured using laser Doppler vibrometry of the piezoelectric stack. (bottom) Generator currents recorded in wild-type and *nompC* mutants in response to a family of piezoelectric step rotations. The stimulus artifact is blanked for clarity.

(D) Average peak generator currents elicited by a family of lateral rotation steps (n = 8 wild-type and 8 *nompC*^{3}/*nompC*^{1}). For submaximal steps, responses in *nompC* mutants are smaller than wild-type. However, the wild-type and mutant response reach the same maximum amplitude.

(E) Average rise time of generator currents versus the amplitude of antennal rotations produced by the piezoelectric probe in the lateral direction. Overall, the rise times in *nompC* mutants are slower than wild-type. However, the rise times are equivalent for the largest steps tested. For all response amplitudes, decay kinetics were systematically faster for *nompC* mutants as compared to wild-type.

In *nompC* mutants, we observed the same process. Although the overall sensitivity of the system was lower in the mutants, the region of maximal sensitivity still migrated by an amount that equal to the magnitude and direction of the static offset (Figures 7C and 7D). These findings demonstrate that NompC is not required for transducer adaptation.

Loss of NompC Leads to Asymmetric Transduction

In addition to the loss of sensitivity in the *nompC* mutant, we noted another striking phenotype: mutant responses lack the bilateral symmetry of wild-type responses. In wild-type recordings, responses to medial and lateral steps were similar in magnitude and kinetics, and both the onset and offset of a step elicited a response (Figure 8A). In *nompC* mutants, responses to medial step rotations less than 10^{-2} radians were systematically smaller than responses to small lateral steps (Figures 8A and 8B).

We saw similar results in response to sound stimuli. During each cycle of a sound stimulus, the antenna rotates both medially and laterally, and so type AB JONs are likely stretched twice per cycle, once medially and once laterally (Figure S2). Consistent with this, sound normally elicits oscillations in the generator current at twice the sound frequency (Figures 8C and 8D). By contrast, in *nompC* mutants, sound elicited oscillations predominantly at the sound frequency, rather than twice this frequency (Figures 8C and 8D).

To see how a small medial-lateral asymmetry can produce a large effect on the dominant frequency of sound responses, it is useful to consider a simple simulation. In this simulation, the relationship between transduction current and rotation is given by a pair of curves —one for medial movement, and the other for lateral movement (Figure 8E). In our simulation, we took the shape of these curves from fits to our data (compare with Figure 7B). We computed the transduction currents at each moment in time as the amount of current specified by these curves, given a sinusoidal stimulus. In JONs, the voltage response to a sound must be a low-pass filtered version of the transduction currents, because of the capacitance of the cell membrane. (Recall that JONs themselves are not voltage-clamped in our recordings; the currents we record are due to voltages propagating through gap junctions into the GFN.) We therefore low-pass filtered the simulated currents.

Our simulations showed that, when the curves are symmetrical around the resting position of the antenna, currents oscillate at twice the frequency of the sound stimulus (Figure 8E). By contrast, when the curves are shifted away from the resting position of the antenna, the dominant frequency of the output signal drops by half, provided that the shift is sufficiently large (Figure 8F). A relatively small shift in the curves (compared to their dynamic range) is required for this behavior. This small shift in the simulated mutant curves mirrors the asymmetry in our mutant data (Figure 7D).

We found that shifting the simulated curves—and also decreasing their steepness—recapitulates the key features of the *nompC* mutant sound responses (Figure 8F). Namely, sound-evoked responses are reduced, the dominant frequency of phasic oscillations drops by half, and the tonic component of the response shrinks relative to the phasic component. In addition, the level of resting current increases, in agreement with the increased rate of spontaneous spiking in the *nompC* mutant data (Figure S3).

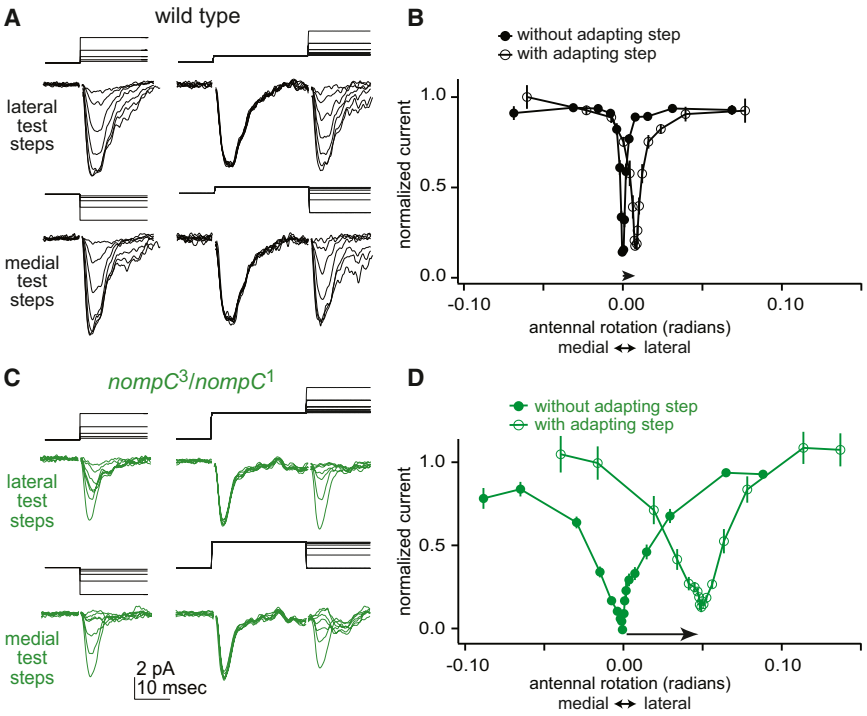

Figure 7. Loss of NompC Does Not Prevent Adaptation to Static Forces

(A) A test step with the piezoelectric probe evokes a transient generator current (left). Next, a static lateral adapting step is applied, followed 27 ms later by another test step to determine the effect of the adapting step (right). The adapting step is 0.0080 radians. Test steps displayed here range from 0.0005 radians to 0.032 radians. Although the adapting step is large enough to produce a nearly saturating transient current, JONs rapidly regain sensitivity to both lateral and medial test steps within 27 ms of the onset of the adapting step.

(B) Peak current averaged across all experiments for each test step amplitude, with and without the adapting step (±SEM; n = 7). Values were normalized to the maximum recorded in that cell. The arrow above the x axis denotes the size and direction of the adapting step. Note that the intersection of the two curves (the position corresponding to minimum current and maximum sensitivity) has adapted to the new position of the antenna.

(C and D) Same as above, but for *nompC* mutant recordings (n = 11). Here the adapting step was larger (0.032 radians) in order to elicit a response to the adapting step that was closer to the wild-type response (compare A and C). The range of test step amplitudes was also extended, again due to the lower overall sensitivity of the mutant responses. Just as in wild-type recordings, the region of maximum sensitivity has adapted to the new position of the antenna. We also saw normal adaptation in the *nompC* mutant when the adapting step was the same size as in (A) and (B) (data not shown).

See also Figure S2.

DISCUSSION

A Sensitive Measure of Auditory Receptor Neuron Activity

In this study, we showed that relatively low-intensity sounds (i.e., lower-intensity than previously used to study courtship behavior) can elicit a behavioral response in *Drosophila*. This provides a motivation for investigating *Drosophila* auditory transduction near absolute threshold and in particular the mechanisms that specify the sensitivity of the transduction complex. This in turn requires developing a sensitive method for measuring transduction currents from type AB JONs, the receptor neurons that are most sensitive to sound (Kamikouchi et al., 2009; Yorozu et al., 2009). Our anatomical and genetic data demonstrate that GFN currents are a selective measure of spiking and generator currents in type AB JONs.

Although this approach involves recording JON activity indirectly via the GFN, the currents we record are nevertheless relatively fast. Indeed, they have latencies and rise times that are similar to (and even faster than) currents that are recorded directly from the cell bodies of mechanosensitive neurons (e.g., Geffeney et al., 2011). Thus, although the signals we record are likely smoothed by cable filtering, the degree of filtering is not necessarily larger than in the case where signals are recorded directly from mechanosensitive neurons. We could observe generator currents in the GFN in response to the smallest step stimulus we used, and this stimulus is essentially identical to the threshold stimulus for evoking calcium responses in JONs (Effertz et al., 2011). The threshold for evoking GFN currents was also essentially the same as the threshold for evoking an antennal nerve field potential response. Finally, these thresholds are just below the threshold for *Drosophila* auditory behavior. Taken together, these comparisons argue that our approach is sensitive enough to report generator currents evoked by near-threshold auditory stimuli.

Properties of Transduction in Auditory Receptor Neurons

Our results confirm and extend what is known about the fundamental properties of transduction in *Drosophila* JONs. First, our measurements show that the transduction complex in type AB JONs is gated by antennal rotations as small as 5×10^{-4} radians. This rotation corresponds to a 74 nm displacement of the distal end of the "lever" (the arista) which projects from the most distal segment of the antenna (see Supplemental Experimental Procedures). This measurement of the transduction threshold is consistent with that obtained by a previous study (Effertz et al., 2011). We should emphasize that the displacement that actually gates the transduction complex is certainly much smaller than this (on the order of a few nm), but because this displacement occurs within the interior of the antenna itself, we cannot measure it directly.

Second, we show that the type AB JONs that provide input to the GFN are depolarized by both lateral and medial rotations.

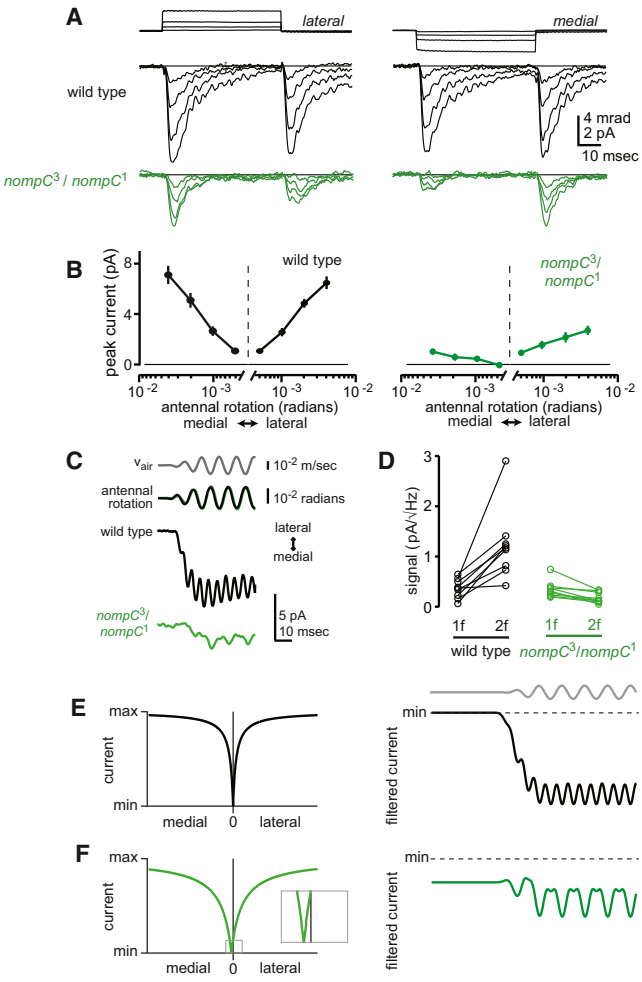

Figure 8. Loss of NompC Impairs the Regulation of Resting Forces on the Transduction Complex

(A) Generator currents evoked in response to a series of step rotations produced by the piezoelectric device (top, largest step is 0.0040 radians). The small oscillations in the wild-type recording after the step are due to resonant movements of the piezoelectric probe, which were observed in the laser Doppler vibrometer measurement of probe displacement (not visible on this scale).

(B) Peak generator currents recorded in wild-type and *nompC* mutant flies in response to small steps (mean ± SEM). In wild-type flies, the point of minimum current matches the resting position of the antenna (indicated by the dashed line). In mutant recordings, it is shifted medially. This is not apparent in Figures 7B and 7C because the scale of that display is linear and compressed (whereas here it is logarithmic and expanded).

(C) A sound stimulus (100 Hz) was presented at an intensity (4.4×10^{-3} m/s, gray trace) that produces antennal movement of similar amplitude in both $nompC^3/nompC^1$ and wild-type antennae (3.9 and 4.1×10^{-3} rad in $nompC^3/nompC^1$ and wild-type, corresponding to the green and black traces). Note that wild-type generator currents (below) oscillate at twice the sound frequency (2f), whereas *nompC* mutant currents oscillate mainly at the sound frequency (1f). Note that $nompC^3/nompC^1$ responses are substantially smaller in the medial direction as compared to the lateral direction.

(D) Group data showing signal strength in the generator currents at 1f and 2f (same stimulus as in E). Most of the signal is 2f in wild-type, but 1f in $nompC^3/nompC^1$. (Increasing sound intensity produced more 2f signal in $nompC^3/nompC^1$; data not shown.) Each symbol represents a different experiment.

(E) Simulated current-rotation curves (left), where zero is the resting position of the antenna. The simulated stimulus is a sinusoidal rotation about the zero point. The simulated current (right), after low-pass filtering, has both a tonic component and a phasic component. The phasic component oscillates at twice the sound frequency.

(F) Same as (E), but with two differences: the curves are shifted slightly to the left (inset), and the curves are less steep. As a result, the simulated current oscillates predominantly at the sound frequency, the tonic component diminishes relative to the phasic component, the overall response magnitude diminishes, and the amount of resting current increases.

See also Figure S3.

Our data suggest that bidirectionality is probably a property of individual JONs of this type, and not just the population as a whole (Figure S2). Indeed, the geometrical arrangement of type A (and perhaps B) JONs within the auditory organ suggests that individual JONs of this type should be stretched by both medial and lateral movements, and thus should respond twice per sound cycle (Kamikouchi et al., 2006).

Finally, we find evidence that some transduction channels are open at rest, even in the absence of sound. This conclusion relies on our observation that JONs spike spontaneously, and that the rate of spontaneous activity is substantially reduced by loss of either Nanchung or Inactive. This conclusion is consistent with previous studies which used other techniques to make inferences about JON activity (Albert et al., 2007; Kamikouchi et al., 2009).

TRPVs as Transduction Complex Components

We have shown that loss of either Nanchung or Inactive abolishes generator currents. Our findings are consistent with previous reports that loss of either Nanchung or Inactive completely eliminates antennal field potential responses to sound (Gong et al., 2004; Kim et al., 2003). However, antennal field potentials are thought to reflect the spiking activity of JONs rather than subthreshold activity (Eberl and Kernan, 2011). Thus, it was not clear from this result whether Nanchung and Inactive were required for transduction or merely spike generation.

Previously, it has been proposed that the role of Nanchung and Inactive is to amplify the transduction signal (Göpfert et al., 2006; Kamikouchi et al., 2009; Lee et al., 2010). However, the latency and speed of the generator currents we record implies that the transduction complex is directly gated by force, rather than gated indirectly by a second messenger. Given this, the Nanchung/Inactive complex is unlikely to merely amplify the transduction signal, because amplification would need to occur within microseconds (which rules out a role for diffusible second messengers), and amplification would need to be >100-fold in magnitude. This level of amplification seems unlikely, given the weak voltage dependence of the channels formed by Nanchung and Inactive (Gong et al., 2004; Kim et al., 2003). Finally, because the Nanchung/Inactive complex does not colocalize with NompC in the JON dendrite (Cheng et al., 2010; Lee et al., 2010; Liang et al., 2011), no amplification mechanism could rely on direct protein-protein interactions between these components.

Given these considerations, it seems more likely that Nanchung and Inactive form part of the transduction complex itself. Consistent with this conclusion, both Nanchung and Inactive confer calcium responses to hypo-osmotic stimuli in

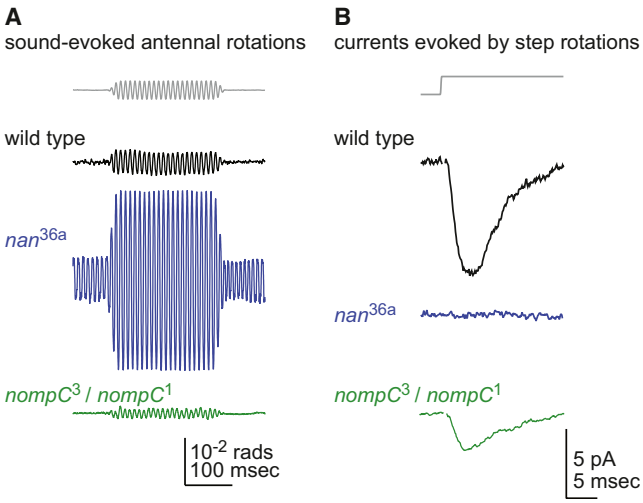

Figure 9. Active Amplification and Auditory Transduction Are Genetically Separable

(A) Sound-evoked antennal rotations for wild-type, *nanchung* mutant, and *nompC* mutant flies. The sound stimulus is shown at top (100 Hz tone, 0.0008 m/s). Antennal movements are larger than normal in the *nanchung* mutant, and reduced in the *nompC* mutant. The active amplification of antennal movement in wild-type and the *nanchung* mutant (relative to the *nompC* mutant) reflects a process which adds mechanical energy to the system (Göpfert et al., 2005) and which is not observed in the *nompC* mutant (Göpfert et al., 2006).

(B) Generator currents recorded in response to a step rotation (10^{-2} radians). Generator currents are absent in the *nanchung* mutant but present in the *nompC* mutant, albeit with less sensitivity to antennal rotation.

See also Figure S4.

heterologous cells (Gong et al., 2004; Kim et al., 2003). However, more work will be needed to test the idea that Nanchung and Inactive could function as force-gated ion channels. An alternative possibility is that Nanchung and Inactive are required for the trafficking or function of an unknown channel.

Previous work has shown that the loss of Nanchung or Inactive results in abnormally large sound-driven antennal movements, as well as spontaneous oscillatory movement in the absence of sound (Göpfert et al., 2006). Our results show that this phenotype goes hand-in-hand with loss of all measurable transduction in JONs (Figure 9). Together, these findings imply that transduction in JONs inhibits the active amplification of antennal movements, possibly because the transduction complex represents a mechanical load on the amplifier element. The presence of active movements in the absence of transduction is also incompatible with the idea that the active amplification of antennal movement is a direct consequence of transduction channel gating.

NompC as a Modulator of Mechanical Forces

Our results demonstrate that NompC is not required for mechanotransduction in the type AB JONs that provide input to the GFN. Moreover, the maximal level of transduction current is essentially normal in the absence of NompC, and the rise time of the current is normal at this maximal level. This result argues that NompC does not specify the intrinsic properties of the transduction channel, such as conductance or ionic selectivity. This result also implies that NompC is not required for the proper trafficking or localization of the transduction complex. These conclusions differ from that of a previous study. That study reported that sound-evoked calcium signals are lost in *nompC* mutant type AB JONs, and concluded that NompC is absolutely required for transduction in these JONs (Effertz et al., 2011). The basis for this discrepancy is not clear, but is likely related to the differences between calcium imaging and electrophysiological recordings. It is possible that the calcium indicator does not report the entirety of the generator current, but rather a small and slow component that does require NompC (Figure S4).

Our results imply that the principal role of NompC is not to transduce force into an electrical signal, but rather to modulate the forces on the transduction complex. Specifically, we find that generator currents are more sensitive to movement when NompC is present, which implies that NompC effectively amplifies mechanical input to the transduction channel, given a fixed amount of antennal movement. Thus, NompC is likely to generate force, or to be permissive for a process that generates force, within the interior of the antenna.

Previous studies have shown that loss of NompC abolishes active amplification of sound-evoked antennal movement, and also reduces spontaneous oscillatory antennal movement (Göpfert et al., 2006; Göpfert and Robert, 2003; see also Figure S1). Thus, loss of NompC appears to eliminate or occlude a process that exerts force on the antenna. This is broadly consistent with our conclusion that NompC is involved in a process which generates force within the interior of Johnston's organ. Recent studies have proposed that NompC is part of the transduction channel, or channel gating spring, or is otherwise required for the function of either of these components (Effertz et al., 2012; Göpfert et al., 2006); however, our observation that transduction persists in the absence of NompC is not consistent with these ideas. Rather, we propose that NompC is permissive for the function of a mechanical amplifier operating between the antennal sound receiver and the transducer. In other words, we propose that the force generated within Johnston's organ is exerted on the transduction apparatus as well as the distal antennal segment.

In addition to amplifying mechanical input to the transduction complex, NompC appears to be required for balancing the medial and lateral resting forces on the transduction complex. In the presence of NompC, JONs are equally sensitive to medial and lateral movements, suggesting that medial and lateral resting forces on the transduction complex are balanced. By contrast, in the absence of NompC, JONs are less sensitive to medial movements than to lateral movements. Our simulations show that this phenotype can result from asymmetrical medial and lateral resting forces on the transduction complex. Thus, a single NompC-dependent process may be responsible for balancing resting forces, as well as actively amplifying stimulus-evoked forces. Adaptation appears to be a separate process, because it does not require NompC.

In sum, we propose that NompC functions in a manner analogous to the role of prestin in the mammalian cochlea (Dallos, 2008). Prestin is expressed by outer hair cells in the cochlea, and is essential for the ability of outer hair cells to

mechanically amplify sound-evoked movements of the basilar membrane. In this manner, prestin increases the sensitivity of the transduction apparatus of the inner hair cells to sound stimuli. However, like NompC, prestin is not absolutely required for transduction, and is not colocalized with the transduction apparatus.

Mechanisms of Force Modulation by NompC

On the basis of its subcellular location, NompC is well-positioned to act as a modulator of mechanical forces. Whereas Nanchung/Inactive are localized to the proximal dendrite, NompC is localized to the distal dendrite, closer to the point where the dendrite inserts into the connective structures that link it to the moving segment of the antenna (Cheng et al., 2010; Gong et al., 2004; Lee et al., 2010; Liang et al., 2011). A bundle of microtubules runs longitudinally through the dendrite (Todi et al., 2004), and this could provide a substrate for adjustments of tension that propagate from the distal to the proximal dendrite. We propose that transduction occurs in the proximal dendritic segment (where Nanchung and Inactive are localized), and this would place NompC in series between the moving segment of the antenna and the transduction complex.

How might NompC be involved in modulating mechanical force? One possibility is that NompC itself generates force that adjusts the longitudinal tension within a JON. NompC contains an unusually large number of ankyrin repeats (Walker et al., 2000). Ankyrin repeats can act as elastic elements, and can generate a refolding force when unfolded (Serquera et al., 2010; Sotomayor et al., 2005). If, for instance, calcium entry into JONs were to modulate the energetics of the unfolded state on a cycle-by-cycle basis, then the refolding force could augment transduction. An alternative possibility is that NompC does not itself generate force, but it is permissive for a process that generates force. For example, calcium influx through NompC might change the state of motor proteins that adjust longitudinal tension within a JON.

Assuming that NompC forms part of a channel, this channel appears to carry relatively little current, or is otherwise ineffective at exciting the JON. We found no detectable generator current in the absence of either Nanchung or Inactive, meaning that any current must be below the limit imposed by noise in our recording. That limit is about 100-fold smaller than the generator currents we measure. Moreover, a previous study reported that sound-evoked calcium signals in JONs are essentially eliminated when Nanchung is absent (Kamikouchi et al., 2009). Together, these findings argue that any ionic flux through NompC is far less than the flux through the transduction complex itself. This conclusion relies on the idea that NompC can still function when Nanchung is absent. In support of this, we have shown that NompC localizes properly in the absence of Nanchung. Moreover, active amplification of antennal movements is intact when Nanchung is absent (Göpfert et al., 2006; see also Figure 9). Because the active amplification of sound-evoked movements requires NompC, this implies that NompC can function without Nanchung. Interestingly, we observe a slow current that persists for hundreds of milliseconds after sound offset, and which absolutely requires both Nanchung and NompC (Figure S4).

Future studies will be required to fully elucidate the mechanism of NompC's action. What makes this mechanism intriguing is the implication there may be two functionally distinct types of TRP channels involved in *Drosophila* hearing (Figure 9). One of these (the transduction channel) evidently carries most or all of the current, and requires Nanchung and Inactive. The other—which requires NompC—carries comparatively little current, and controls the active generation of force within the auditory organ.

EXPERIMENTAL PROCEDURES

Procedures are summarized below; see Supplemental Experimental Procedures for details on all sections.

Fly Stocks and Genetic Manipulations

Fly stocks and genetic manipulations were as follows:

Figures 1B–1D, "Dickinson wild-caught"
Figure 1E, *G0117-Gal4,UAS-CD8:GFP/UAS-dicer2;+/+;UAS-DmNa$_v$-RNAi/+* (control) and *G0117-Gal4,UAS-CD8:GFP/UAS-dicer2;nan-Gal4/+;UAS-DmNa$_v$-RNAi/+* (knockdown)
Figures 1F and 1G, *G0117-Gal4,UAS-CD8:GFP*
Figures 2B, 2C,and 2F, *G0117-Gal4,UAS-CD8:GFP*
Figures 2D and 2E, *G0117-Gal4,UASDC8:GFP* (pharmacology) and *shakB^2;G0066-Gal4,UAS-CD8:GFP/+* (*shakB^2*) and *G0117-Gal4,UAS-CD8:GFP/UAS-dicer2;nan-Gal4/+,UAS-DmNa$_v$-RNAi/+* (knockdown).
Figure 3, *G0117-Gal4,UAS-CD8:GFP*
Figures 4A–4D, *G0117-Gal4,UAS-CD8:GFP;+/+;nan^{36a}* and *iav^1;G0066-Gal4,UAS-CD8:GFP/+*
Figure 4E, +;UAS-*nompC-L:GFP/nan-Gal4;nan^{36a}* and +;*UAS-nompC-L:GFP/nan-Gal4;+/nan^{36a}*
Figure 5A, *JO-CE-Gal4/+;UAS-CD8:GFP/+* and *UAS-CD8:GFP/JO-AB-Gal4*
Figures 5B and 5C, *JO-CE-Gal4* or *JO-AB-Gal4* (wild-type) and *iav^1;+/+;UAS-iav/+* (*iav^1*) and *iav^1;nan-Gal4/+;UAS-iav/+* (*iav* rescue in all JONs) and *iav^1;+/+;UAS-iav/JO-AB-Gal4* (*iav* rescue type AB) and *iav^1;JO-CE-Gal4/+;UAS-iav/+* (*iav* rescue type CE)
Figures 6, 7, and 8, *G0117-Gal4,UAS-CD8:GFP* (wild-type) and *G0117-Gal4,UAS-CD8:GFP;nompC^3,cn,bw/nompC^1,cn,bw*
Figure 9, *G0117-Gal4,UAS-CD8:GFP* (wild-type), and *G0117-Gal4,UAS-CD8:GFP;+/+;nan^{36a}* and *G0117-Gal4,UAS-CD8:GFP;nompC^3,cn,bw/nompC^1,cn,bw*

Sound Measurement, Isolation, and Delivery

Sound particle velocities were measured using a calibrated pressure gradient microphone. All electrophysiological, behavioral, and laser Doppler vibrometry recordings were made in a sound isolation chamber which reduced background noise to 23 dB SPL (unweighted). The duration of the tone was 250 ms, and the first and last 10% of the stimulus was cosine theta squared ramped. The speaker was ~230 mm from the fly.

Behavioral Experiments

The fly was glued to a tether that was positioned above a ball floating on a cushion of air. The fly's locomotion was recorded by measuring the motion of the ball using an optical mouse sensor below the ball.

Antennal Nerve Field Potential Recordings

Field potential recordings were performed using a saline-filled quartz electrode. The electrode was inserted between the first and second antennal segments.

Laser Doppler Vibrometry

Sound-driven antennal movements were measured using a laser Doppler vibrometer with the laser spot focused on the most distal branch point of

the lever-like structure (the arista) which protrudes from the most distal antennal segment (Figure S1). The laser beam was positioned orthogonal to the plane of the arista, and so our measurements quantified the displacement of the arista along this axis. Measurements of aristal displacement were converted into measurements of aristal rotation by measuring the distance from the laser spot on the arista to the midline of the distal (third) antennal segment, and then taking the small angle approximation. The arista is rigidly coupled to the distal antennal segment, and so aristal and antennal rotation are the same. We report rotation (rather than antennal displacement) because this measure should not depend on the position of the laser measurement spot on the arista.

Whole-Cell Recordings

Currents were recorded from the Giant Fiber Neuron (GFN) in vivo in whole-cell voltage-clamp mode under visual control on an upright compound microscope. The fly was suspended in a piece of titanium foil such that the upper side of the fly's head was bathed in oxygenated saline, while the lower side of the head and both antennae remained dry. The GFN was identified based on GFP expression under the control of the *G0117-Gal4* or *G0066-Gal4* lines.

Immunohistochemistry

See Supplemental Experimental Procedures.

Piezoelectric Antennal Movement

The second antennal segment was glued to the titanium foil, leaving only the distal (third) antennal segment free to rotate. A piezoelectric stack was used to rotate the third antennal segment via a tungsten probe attached to the arista. Laser Doppler vibrometry was used to measure the displacement of the piezoelectric stack. These measurements showed that the rise time of step stimuli (from 10% of maximum to 90% of maximum) was 300–400 μs. The tip of the tungsten probe was placed on the distal-most branch point of the arista, the same location targeted in the laser Doppler vibrometry measurements (Figure S1). The measured displacements of the probe (and thus the arista) were converted to rotations by measuring the length of the arista (Figure S1).

Data Analysis and Simulations

See Supplemental Experimental Procedures.

SUPPLEMENTAL INFORMATION

Supplemental Information includes four figures and Supplemental Experimental Procedures and can be found with this article online at http://dx.doi.org/10.1016/j.neuron.2012.11.030.

ACKNOWLEDGMENTS

We thank John Assad, David Corey, Barry Dickson, Tom Middendorf, Daniel Robert, Bernardo Sabatini, Gary Yellen, and members of the Wilson lab for helpful comments throughout the project. Elizabeth Hong provided expert advice. The following individuals kindly supplied us with flies (see Supplemental Experimental Procedures for original citations): "Dickinson wild-caught" stock (Michael Dickinson), *iav*^{1} and *UAS-iav* (Craig Montell), *UAS-dicer2* (Heather Broihier), *JO-AB-Gal4* and *JO-CE-Gal4* (David Anderson), *nompC*^{3}, *nompC*^{1}, and *UAS-nompC-L:GFP* (Yuh-Nung Jan), *nan-Gal4* (Larry Zipursky), and *shakB*^{2} (Robert Wyman). This work was supported by a Program Grant from the Human Frontiers Science Program. R.I.W. is an HHMI Early Career Scientist. B.P.L. and A.E.B. were supported by National Science Foundation Graduate Research Fellowships. Additional support to B.P.L. was provided by the Sault Ste. Marie Tribe of Chippewa Indians Self-sufficiency Fund. B.P.L. and R.I.W. designed the experiments, except for the behavioral experiments, which were designed by A.E.B. and R.I.W. B.P.L. performed the experiments and analyzed the data, except for Figures 1A–1D, where the experiments and analyses were performed by A.E.B. with assistance from Q.G. B.P.L. and R.I.W. wrote the paper. A.-S.C. provided the *G0117-Gal4* and *G0066-Gal4* lines.

Accepted: November 28, 2012
Published: January 9, 2013

REFERENCES

Albert, J.T., Nadrowski, B., and Göpfert, M.C. (2007). Mechanical signatures of transducer gating in the *Drosophila* ear. Curr. Biol. *17*, 1000–1006.

Cheng, L.E., Song, W., Looger, L.L., Jan, L.Y., and Jan, Y.N. (2010). The role of the TRP channel NompC in *Drosophila* larval and adult locomotion. Neuron *67*, 373–380.

Curtin, K.D., Zhang, Z., and Wyman, R.J. (2002). Gap junction proteins expressed during development are required for adult neural function in the Drosophila optic lamina. J. Neurosci. *22*, 7088–7096.

Dallos, P. (2008). Cochlear amplification, outer hair cells and prestin. Curr. Opin. Neurobiol. *18*, 370–376.

Eberl, D.F., and Kernan, M.J. (2011). Recording sound-evoked potentials from the Drosophila antennal nerve. Cold Spring Harb. Protoc. 2011, prot5576.

Eberl, D.F., Duyk, G.M., and Perrimon, N. (1997). A genetic screen for mutations that disrupt an auditory response in Drosophila melanogaster. Proc. Natl. Acad. Sci. USA *94*, 14837–14842.

Eberl, D.F., Hardy, R.W., and Kernan, M.J. (2000). Genetically similar transduction mechanisms for touch and hearing in Drosophila. J. Neurosci. *20*, 5981–5988.

Effertz, T., Wiek, R., and Göpfert, M.C. (2011). NompC TRP channel is essential for *Drosophila* sound receptor function. Curr. Biol. *21*, 592–597.

Effertz, T., Nadrowski, B., Piepenbrock, D., Albert, J.T., and Göpfert, M.C. (2012). Direct gating and mechanical integrity of Drosophila auditory transducers require TRPN1. Nat. Neurosci. *15*, 1198–1200.

Fettiplace, R., and Ricci, A.J. (2003). Adaptation in auditory hair cells. Curr. Opin. Neurobiol. *13*, 446–451.

Geffeney, S.L., Cueva, J.G., Glauser, D.A., Doll, J.C., Lee, T.H., Montoya, M., Karania, S., Garakani, A.M., Pruitt, B.L., and Goodman, M.B. (2011). DEG/ENaC but not TRP channels are the major mechanoelectrical transduction channels in a *C. elegans* nociceptor. Neuron *71*, 845–857.

Gong, Z., Son, W., Chung, Y.D., Kim, J., Shin, D.W., McClung, C.A., Lee, Y., Lee, H.W., Chang, D.J., Kaang, B.K., et al. (2004). Two interdependent TRPV channel subunits, inactive and Nanchung, mediate hearing in Drosophila. J. Neurosci. *24*, 9059–9066.

Göpfert, M.C., and Robert, D. (2001). Biomechanics. Turning the key on Drosophila audition. Nature *411*, 908.

Göpfert, M.C., and Robert, D. (2002). The mechanical basis of Drosophila audition. J. Exp. Biol. *205*, 1199–1208.

Göpfert, M.C., and Robert, D. (2003). Motion generation by Drosophila mechanosensory neurons. Proc. Natl. Acad. Sci. USA *100*, 5514–5519.

Göpfert, M.C., Humphris, A.D., Albert, J.T., Robert, D., and Hendrich, O. (2005). Power gain exhibited by motile mechanosensory neurons in Drosophila ears. Proc. Natl. Acad. Sci. USA *102*, 325–330.

Göpfert, M.C., Albert, J.T., Nadrowski, B., and Kamikouchi, A. (2006). Specification of auditory sensitivity by Drosophila TRP channels. Nat. Neurosci. *9*, 999–1000.

Hudspeth, A.J. (2008). Making an effort to listen: mechanical amplification in the ear. Neuron *59*, 530–545.

Inagaki, H.K., Kamikouchi, A., and Ito, K. (2010). Protocol for quantifying sound-sensing ability of Drosophila melanogaster. Nat. Protoc. *5*, 26–30.

Kamikouchi, A., Shimada, T., and Ito, K. (2006). Comprehensive classification of the auditory sensory projections in the brain of the fruit fly Drosophila melanogaster. J. Comp. Neurol. *499*, 317–356.

Kamikouchi, A., Inagaki, H.K., Effertz, T., Hendrich, O., Fiala, A., Göpfert, M.C., and Ito, K. (2009). The neural basis of Drosophila gravity-sensing and hearing. Nature *458*, 165–171.

Kang, L., Gao, J., Schafer, W.R., Xie, Z., and Xu, X.Z. (2010). *C. elegans* TRP family protein TRP-4 is a pore-forming subunit of a native mechanotransduction channel. Neuron *67*, 381–391.

Kazama, H., and Wilson, R.I. (2008). Homeostatic matching and nonlinear amplification at identified central synapses. Neuron *58*, 401–413.

Kernan, M.J. (2007). Mechanotransduction and auditory transduction in Drosophila. Pflugers Arch. *454*, 703–720.

Kim, J., Chung, Y.D., Park, D.Y., Choi, S., Shin, D.W., Soh, H., Lee, H.W., Son, W., Yim, J., Park, C.S., et al. (2003). A TRPV family ion channel required for hearing in Drosophila. Nature *424*, 81–84.

Lee, J., Moon, S., Cha, Y., and Chung, Y.D. (2010). Drosophila TRPN(=NOMPC) channel localizes to the distal end of mechanosensory cilia. PLoS ONE *5*, e11012.

Liang, X., Madrid, J., Saleh, H.S., and Howard, J. (2011). NOMPC, a member of the TRP channel family, localizes to the tubular body and distal cilium of Drosophila campaniform and chordotonal receptor cells. Cytoskeleton *68*, 1–7.

Menda, G., Bar, H.Y., Arthur, B.J., Rivlin, P.K., Wyttenbach, R.A., Strawderman, R.L., and Hoy, R.R. (2011). Classical conditioning through auditory stimuli in Drosophila: methods and models. J. Exp. Biol. *214*, 2864–2870.

Nadrowski, B., Albert, J.T., and Göpfert, M.C. (2008). Transducer-based force generation explains active process in *Drosophila* hearing. Curr. Biol. *18*, 1365–1372.

Nagel, K.I., and Wilson, R.I. (2011). Biophysical mechanisms underlying olfactory receptor neuron dynamics. Nat. Neurosci. *14*, 208–216.

Phelan, P., Nakagawa, M., Wilkin, M.B., Moffat, K.G., O'Kane, C.J., Davies, J.A., and Bacon, J.P. (1996). Mutations in shaking-B prevent electrical synapse formation in the Drosophila giant fiber system. J. Neurosci. *16*, 1101–1113.

Robert, D., and Hoy, R.R. (2007). Auditory systems in insects. In Invertebrate Neurobiolology, G. North and R.J. Greenspan, eds. (Cold Spring Harbor, NY: Cold Spring Harbor Laboratory Press), pp. 155–184.

Serquera, D., Lee, W., Settanni, G., Marszalek, P.E., Paci, E., and Itzhaki, L.S. (2010). Mechanical unfolding of an ankyrin repeat protein. Biophys. J. *98*, 1294–1301.

Sivan-Loukianova, E., and Eberl, D.F. (2005). Synaptic ultrastructure of Drosophila Johnston's organ axon terminals as revealed by an enhancer trap. J. Comp. Neurol. *491*, 46–55.

Sotomayor, M., Corey, D.P., and Schulten, K. (2005). In search of the hair-cell gating spring elastic properties of ankyrin and cadherin repeats. Structure *13*, 669–682.

Strausfeld, N.J., and Bassemir, U.K. (1983). Cobalt-coupled neurons of a giant fibre system in Diptera. J. Neurocytol. *12*, 971–991.

Todi, S.V., Sharma, Y., and Eberl, D.F. (2004). Anatomical and molecular design of the Drosophila antenna as a flagellar auditory organ. Microsc. Res. Tech. *63*, 388–399.

Tootoonian, S., Coen, P., Kawai, R., and Murthy, M. (2012). Neural representations of courtship song in the Drosophila brain. J. Neurosci. *32*, 787–798.

von Schilcher, F. (1976). The role of auditory stimuli in the courtship of *Drosophila melanogaster*. Anim. Behav. *24*, 18–26.

Walker, R.G., Willingham, A.T., and Zuker, C.S. (2000). A Drosophila mechanosensory transduction channel. Science *287*, 2229–2234.

Yorozu, S., Wong, A., Fischer, B.J., Dankert, H., Kernan, M.J., Kamikouchi, A., Ito, K., and Anderson, D.J. (2009). Distinct sensory representations of wind and near-field sound in the Drosophila brain. Nature *458*, 201–205.